Tropical Intraseasonal Oscillation, Super Cloud Clusters, and Cumulus Convection Schemes

WINSTON C. CHAO

Laboratory for Atmospheres, NASA/Goddard Space Flight Center, Greenbelt, Maryland

SHIAN-JIANN LIN

General Sciences Corporation, Laurel, Maryland

(Manuscript received 30 April 1993, in final form 7 September 1993)

ABSTRACT

A new framework for interpreting the origin of the tropical intraseasonal oscillation (TISO), which avoids the speed and scale selection problems in the previous theories, is proposed in this study. In this interpretation TISO is viewed as an oscillation driven by an eastward moving convective region. This convective region consists of one or more super cloud clusters originating in the Indian Ocean and terminating in mid-Pacific, and is then followed by another convective region arising in the Indian Ocean in a period of 40–50 days. Additionally, a formal analogy is pointed out between super cloud clusters and the middle-latitude baroclinic wave packets.

This study includes a simulation of TISO in a 2D model to support our interpretation. Experiments were conducted with four different convection schemes. The authors advocate that the successful simulation of TISO depends on the successful simulation of super cloud clusters, which in turn depends on the successful simulation of the life cycle of cloud clusters, which further in turn depends on the choice of cumulus convection scheme. What makes a cumulus convection scheme successful in simulating TISO is discussed.

1. Introduction

The tropical intraseasonal oscillation (TISO) (Madden and Julian 1971, 1972; Madden 1986; Murakami and Nakazawa 1985; among others) has thus far no well-accepted theory [for a recent review see Hayashi and Golder (1993)]. The frequently discussed wave–CISK mechanism (Chao 1987; Lau and Peng 1987; Miyahara 1987; Hendon 1988; Chang and Lim 1988; Wang 1988) has the major difficulty of too high eastward speed. Most wave–CISK type simulations give a period of 20–30 days for the convective region to circle the earth. To reduce the speed of the oscillation, the height of the maximum cumulus heating must be lowered to the lower troposphere (Takahashi 1987; Lau et al. 1989), a disagreement with observations. Also, many studies have the implicit assumption that the precipitation region circles the globe in about 45 days. This assumption is in conflict with the observations. The precipitation region associated with the TISO travels only one-third of the globe, from the Indian Ocean to mid-Pacific, in about 45 days (and then a new convective region starts in the Indian Ocean), a much slower speed [see Lau and Chen (1986), including the cover picture]. This fact puts the wave–CISK mechanism in further doubt as a valid explanation for TISO. The circulation fields associated with this moving convective region have a global scale and of course the same period. Thus, when the circulation fields are analyzed, one gets a picture of a global-scale traveling mode circulating the whole globe with a 40–50-day period.

Another serious difficulty with the wave–CISK mechanism lies in the fact that its most favored scale of convective region is the smallest in a model. The methods of getting around this difficulty (e.g., Wang and Chen 1989; Wang and Rui 1990) have not been validated in models. However, we should point out that the scale selection problem exists mostly in linear models (with or without conditional heating) and some nonlinear models do not have this problem (Hayashi and Sumi 1986). Nevertheless, even if scale selection does not present a problem, the excessive speed problem alone can invalidate wave–CISK.

The evaporation–surface wind feedback mechanism, which was later renamed as the wind-induced surface heat exchange (WISHE) mechanism (Emanuel 1987; Neelin et al. 1987), also suffers from the scale selection difficulty. Although there has been an attempt to resolve this difficulty (Yano and Emanuel 1991),

Corresponding author address: Dr. Winston C. Chao, Code 913, NASA/GSFC, Greenbelt, MD 20771.

the proposed resolution has yet to be tested in global models. Additionally, Neelin et al. (1987) showed that when WISHE is suppressed in their model, the same oscillation can still occur but with much weaker amplitude.

Furthermore, the link between wave–CISK and WISHE on the one hand and the more recent observational findings on the other has not been established. These observational findings (Nakazawa 1988; Lau et al. 1991; Sui and Lau 1992) show that the convective region associated with the TISO consists of one or more super cloud clusters and within each super cloud cluster individual cloud clusters arise, move westward, and then decay within 2 to 3 days. New cloud clusters appear to the east of the existing cloud clusters. The envelope of the cloud clusters is the super cloud cluster, which moves eastward.

In this paper we propose a radically different explanation for the origin of the TISO. Our explanation depicts the TISO as the result of a convective region moving eastward starting from the Indian Ocean and ending in mid-Pacific, apparently due to the fact that the lower SST in the eastern Pacific can no longer sustain it. In El Niño years when warm SST extends into the eastern Pacific, this convective region can move into the eastern Pacific. The speed of the movement is not always very steady. Once this convective region ends in mid-Pacific, another one starts in the Indian Ocean. The cycle repeats in 40–50 days. This part of the explanation is really nothing more than a summary of recent satellite observations. The global-scale wind circulation in TISO as a response to the heating inside this convective region has a Kelvin wave structure ahead of the convective region and a Rossby wave structure behind it. This circulation response part of the explanation is also not new. It has been proposed by Yamagata and Hayashi (1984) and Chao (1987) and has been demonstrated by observations (e.g., Nogues-Paegle et al. 1989). Recent satellite observations have demonstrated that this convective region is composed of one or more super cloud clusters (e.g., Nakazawa 1988). What has not been explained thus far is the origin of this convective region, its internal structure, size, and speed ($\sim$3.5 m s^{-1}). Its speed is the most important thing to understand, since it is at the core of understanding the 40–50-day period.

In our interpretation, the super cloud clusters and their eastward movement originate from what we shall call *the cloud cluster teleinduction mechanism* of initiating a new cloud cluster by an existing cloud cluster at a distance (800–1200 km) to its east. Locations close to the existing cloud cluster, because of the compensating downward motion associated with the existing cloud cluster, are not favorable for the emergence of a new cloud cluster. The reason the eastern side of an existing cloud cluster is more favorable than the western side for the new cloud cluster to emerge has to do with basic flow in the boundary layer being easterly, which is also strengthened by the circulation induced by the existing cloud cluster. In other words, the east side is where the main moisture supply is coming from. Once the new cloud cluster emerges, it competes for moisture supply with the existing cloud cluster. Since the moisture supply comes mainly from the east in the tropical easterly basic flow environment, the new cloud cluster has the first chance in harnessing it. Losing the competition, the existing cloud cluster, while moving westward (the reason for the westward movement will be discussed in section 3), soon decays. The successive generation of new cloud clusters in the east and the subsequent decay of existing ones give rise to an eastward moving envelope, which is the super cloud cluster. The speed of the super cloud cluster is determined by the westward speed of the cloud cluster, the distance between the cloud clusters, and the frequency of generation of new cloud clusters. Often there can be more than one super cloud cluster in the convective region associated with the TISO (Nakazawa 1988). This, along with the origin of the cloud cluster teleinduction mechanism—that is, why new cloud clusters should emerge at all—will be explained in section 4.

The basic ideas in wave–CISK and WISHE do play important roles, in our interpretation, on the temporal and spatial scales of the cloud clusters and some supporting role on the scale of super cloud clusters. The term "CISK" has different meanings to different people. Here we will confine ourselves to its most basic meaning: the cooperation between convective heating and the heating-induced low-level moisture convergence through surface friction. The term "wave–CISK" means that the low-level convergence through surface friction in CISK is replaced by convergence of the wave (or the circulation field) excited by the convective heating. When wave–CISK is operating, there is no doubt that WISHE is playing a role. Wave–CISK is responsible for the growth of a cloud cluster (this point will be further discussed shortly) but not its initiation. The initiation of a cloud cluster has to rely on the circulation field induced by an existing (and evolving) cloud cluster 800–1200 km to the west, when the basic flow is easterly. The existing cloud cluster is also responsible for creating the favorable condition for the new cloud cluster to rise. So there is no doubt about the existence of the cloud cluster teleinduction mechanism. In other words, wave–CISK is an instability responsible for the growth of a cloud cluster, and the cloud cluster teleinduction is the mechanism that brings the dynamical and thermodynamical fields at a particular location toward (and provides the final push to cross over) the critical point beyond which the wave–CISK instability (or a new cloud cluster) starts.

Thus, in our view wave–CISK operates only at the scale of cloud cluster. Also, the "wave" involved is nothing more than the circulation associated with a

cloud cluster. Such a wave is composed of upward motion of cloud cluster scale generated by buoyancy and compensating downward motion outside the cloud cluster, and the only label that can be attached to it is gravity wave. This is entirely different from the previous theories, which associate wave–CISK (invoking global-scale Kelvin and Rossby waves) directly with the global scale of the TISO itself. Of course, when the convective region associated with TISO is viewed as a whole, there is heating in this region and convergence into it in the boundary layer giving the appearance of wave–CISK, whose importance was misplaced by previous theories. The "wave" associated with super cloud clusters has a scale large enough to be affected by earth's rotation and can be labeled as a mixture of gravity, Rossby, and Kelvin waves.

Pushing the above discussion further down the scale, we may argue that the true wave–CISK operates at cloud scale only. The wave–CISK associated with a cloud cluster is only an appearance. Like the super cloud clusters, which owe their existence to the nonlinear interaction among cloud clusters, cloud clusters depend on the nonlinear interaction among clouds; that is, the initiation of one cloud depends on the circulation field associated with an existing cloud. Wave–CISK is a concept that does not address the nonlinear scale interaction and the nonlinear interaction among entities of the same scale that lie at the core of many tropical phenomena (TISO, in particular). Thus, it is not surprising that studies of TISO based on the wave–CISK concept are plagued with problems.

In this work, we advocate that the successful simulation of TISO depends on the successful simulation of the super cloud clusters, which in turn depends on the successful simulation of the life cycle of cloud clusters and the cloud cluster teleinduction mechanism. This paper presents a modeling effort to investigate the super cloud clusters and the TISO with the goal of a better understanding and with the expectation that such understanding will contribute to the GCM simulation of TISO.

We will use a two-dimensional model covering the vertical plane along the equator for this study. The main advantages of the 2D model are its ease of use, relative ease in interpretation, and complementary role to the 3D models. It is certainly an important member of a hierarchy of models that are necessary in the investigation. The model (section 2) is reduced from the Goddard Laboratory for Atmospheres General Circulation Model (GLA GCM). S.-J. Lin has designed a simple convection scheme for this investigation. In addition, the relaxed Arakawa–Schubert (RAS) convection scheme (Moorthi and Suarez 1992) that comes with the model, the Emanuel (1991) scheme, and the moist convective adjustment scheme (Manabe 1965) are used (section 3) to demonstrate that the successful simulation of the super cloud clusters and thus the TISO depends critically on the type of convection scheme used. The roles of the Coriolis force, basic wind, and SST distribution are also investigated. What distinguishes the successful cumulus schemes from the unsuccessful ones is discussed in section 4. We will also discuss the origin of the super cloud clusters, which drives TISO. Summary and remarks are given in the final section.

2. A 2D model

The model used is reduced from the GLA GCM, which is a substantially revised version of the original GLAS fourth-order model (Kalnay et al. 1983). The model applies a center fourth-order differencing scheme on the (nonstaggered) A grid in the horizontal, and a second-order differencing scheme in the vertical. The flux-form spatial finite-differencing scheme formally conserves kinetic energy but not potential enstrophy. However, potential enstrophy is nearly conserved in practice. The vertical finite-differencing scheme is that of Arakawa and Suarez (1983). As dictated by that scheme, potential temperature (instead of temperature) is used as a prognostic variable. The locally consistent hydrostatic equation at the bottom level is an important feature of this scheme. The time differencing is an initial Matsuno step followed by leapfrog steps. A fourth-order Shapiro filter is applied to momentum and potential temperature.

The moisture transport utilizes a second-order van Leer–type scheme, which is conservative and monotonic [see Lin et al. (1994) for details]. The monotonic constraint on the implied subgrid moisture distribution guarantees the positivity of the water vapor mixing ratio without the need for an explicit diffusion (such as the Shapiro filter in the original design) and/or filling algorithm. Transport of moisture is done sequentially in each spatial direction. Since there is no need for spatial and time filters, this new scheme is just as fast as the original fourth-order finite-difference scheme on the CRAY-YMP. A detailed comparison is presented in Lin et al. (1994).

The planetary boundary layer and vertical diffusion parameterizations follow those of the European Centre for Medium-Range Weather Forecasts General Circulation Model (Louis 1979). It uses the Monin–Obukhov similarity theory for surface fluxes calculation. The bottom layer is treated as the planetary boundary layer. Vertical diffusion coefficient is Richardson number dependent. For our limited modeling purpose, the observed zonally averaged net radiative heating (Newell et al. 1972) is used in lieu of the costly radiation parameterization.

The 2D model is basically a longitude–height model at a chosen latitude covering half the globe over ocean only. When the chosen latitude is the equator, meridional velocity v is set to zero and there is no meridional

pressure gradient force; otherwise v is allowed to vary in time and space and a zonally uniform meridional pressure gradient force is imposed as will be described later. There are 17 sigma layers, as in the original settings (Fox-Rabinovitz et al. 1991), with the top four layers in the stratosphere and the bottom three layers below 900 mb. The horizontal grid size is 1 degree. Cyclic boundary conditions are used. The time step is 2.5 minutes. The SST is set at 28°C in the left one-third of the domain and at 30°C in the remaining domain. The purpose of such setting is to provide an environment for the initiation and termination of the super cloud clusters. Observations show that the super cloud clusters start in the Indian Ocean and terminate in mid-Pacific or eastern Pacific in the El Niño years. To maintain the easterly basic wind one of two methods is used. The first method simply restores the zonally averaged (on sigma surface) u wind to a preset vertical wind profile at every time step. The second method uses a Rayleigh-type friction to relax the zonally averaged u wind toward a preset vertical wind profile with a time scale of 3 days. The preset vertical wind profile in both methods is simply a constant (-5 and -10 m s^{-1}, respectively) with no vertical shear. These methods are to simulate the convergence (or divergence) of meridional eddy momentum flux, which maintains the zonal mean wind at the simulated latitude.

To demonstrate the sensitivity of the model results to various cumulus convection schemes, we will use the relaxed Arakawa–Schubert scheme (Moorthi and Suarez 1992), the Emanuel scheme (1991), the moist convective adjustment scheme (as used in the GFDL model), and a scheme that S.-J. Lin designed, which is an intuitively simple, yet realistic in some aspects, moist convection scheme (SCS hereafter). A brief description of SCS design follows.

In SCS we first compute a *reference* water vapor mixing ratio profile in the following manner. Starting from the bottom layer of each column the moist static energy of the layer $h_k = C_pT_k + \Phi_k + Lq_k$, where Φ is the geopotential and L is the latent heat, is compared with the saturation moist static energy $h^*_{k-1} = C_pT_{k-1} + \Phi_{k-1} + Lq^*_{k-1}$ of the layer immediately above. If $h_k > h^*_{k-1}$, that is, when *local* moist convective potential energy is available, an approximate amount of excess water substance, which is less than the maximum allowable amount, $W = (h_k - h^*_{k-1})M_k/L$, where M_k is the mass in the lower-layer grid box, is transported upward from layer k to layer $k - 1$. Note that the latent heat constant L is just the latent heat of condensation if the temperature in the lower layer is above freezing; it is the sum of the latent heat of fusion and condensation if the temperature is below freezing. The updated q_{ref} at layer $k - 1$ is then used in the continued comparison with the layer above. If the above convective instability criterion is not met, then the upward convective transport of water substance is assumed to terminate right there; but the comparison continues for the next higher layer. This layer by layer adjustment of the moisture mixing ratio continues until the top layer is reached, and a final reference profile q_{ref} is obtained. Note that the upward moisture transport (by the unspecified subgrid scale drafts) can initiate from any layer and end at any layer above. In other words, the cloud base can be at any level, and the possibility of multiple cloud bases is not ruled out.

Once the reference mixing ratio profile is obtained, starting from the top layer, the increase in water vapor $dq_k = q_{\text{ref}} - q_{\text{original}}$ at layer k is partitioned into two parts. The first part (a small constant, set to a maximum of 10% for our chosen horizontal resolution) is used to moisten the layer, but not to supersaturate the layer. The remaining part is converted into convective rain. No moistening is allowed if the original profile is supersaturated, and all of the moisture increase is relegated as convective rain in that case. The latent heat of condensation associated with the production of convective rain is then released to increase T_k. Subsequently, if T_k is below freezing, a fraction of the rain is frozen (which may become any solid water substance, e.g., snow, ice, and hail) and the latent heat of fusion is released to warm the layer. Otherwise, if T_k is greater than the freezing point and there is solid water substance (received from layers above) present, a fraction of that solid water is melted, which is then added to the rainwater budget in that layer. This is followed by the computation of evaporation of convective rainwater. The rain reevaporation rate was computed by the simplified form of Emanuel [his Eq. (12b), 1991] and the terminal velocity is assumed to be a constant (0.45 mb s^{-1}). The evaporation increases q_k and decreases T_k while conserving h_k. The convective rain and solid water are then delivered to the next lower layer and the computation continues until the bottom layer is reached. The sum of rainwater and solid water reached and remained in the bottom layer is the net convective precipitation. Before the computation of the large-scale precipitation, this whole process is iterated (at most three times) to prevent over- and/or underremoval of the convective instability. The computation of large-scale precipitation and rain reevaporation is similar to those of Sud and Molod (1988), except that the freezing and melting processes are included, in a fashion similar to that of the convective process.

This scheme outputs the final temperature, water vapor mixing ratio profiles, and the net precipitation. But instead of an instantaneous adjustment to the final profiles, the differences between the final and initial profiles are used to compute the heating/cooling and drying/moistening rates. Since no convective rain can be generated in the bottom layer, heating due to moist process in the bottom layer can only come from large-scale condensation and/or freezing of the rainwater, which

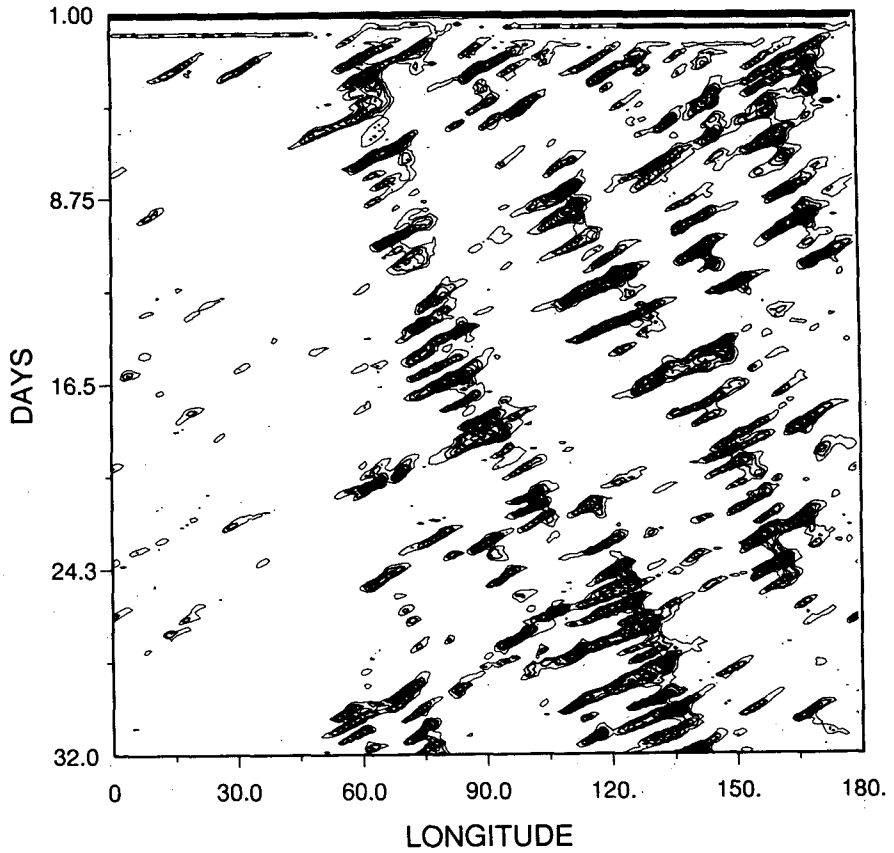

FIG. 1. Time–longitude distribution of precipitation in the control experiment (in mm day^{-1}). The 3-hourly accumulated precipitation was used in plotting. Contour interval is 5 mm day^{-1}.

do occur in nature. The design philosophy of this scheme is to keep the parameterization of unresolvable processes, which are not well understood either from theory or observations, as simple and as explicit as possible. Any physical process that can be treated explicitly, such as freezing and melting of the water substance, should be treated so. The treatment of those unresolvable subgrid-scale drafts should be done as simply and as little as possible to avoid too strong and likely inaccurate interference with the physics and dynamics of the resolvable processes. Those unspecified but implicitly present subgrid-scale drafts serve, in this simple scheme, mainly as agents of the upward transport of moisture, whose purpose is to release the local grid-scale convective instability of the resolvable motions. This scheme is vectorizable on the CRAY-YMP. In the tests we have done, this scheme is about 5 to 10 times faster than the relaxed Arakawa–Schubert scheme coupled with a similarly formulated rain reevaporation routine (Sud and Molod 1988).

The heating, moistening, and momentum change rates from the physics package are multiplied by the dynamics time step, and the products are added to the respective prognostic quantities every dynamics time step. The rates are updated at different intervals. The radiation rates are fixed. For the turbulence and boundary-layer parameterization, the rates are updated every 15 minutes. For convection the rates are updated at different intervals for different convection schemes. We used a 9-minute interval for the relaxed Arakawa–Schubert scheme, 15-minute interval for the Emanuel scheme, and 1-hour interval for both the GFDL scheme and the SCS.

3. Experiments

The model initial conditions are specified in a simple manner: v is set to be zero, u is a constant easterly of 10 m s^{-1} everywhere, and T is zonally uniform and varies from 300 K at the bottom to 220 K at the top linearly in sigma. Relative humidity is also zonally uniform with values set somewhat arbitrarily to be sigma. Surface pressure is a Gaussian hump of 10-mb amplitude and a width of 8° in longitude centered over the middle of the domain and superimposed on a zonally uniform value of 1000 mb.

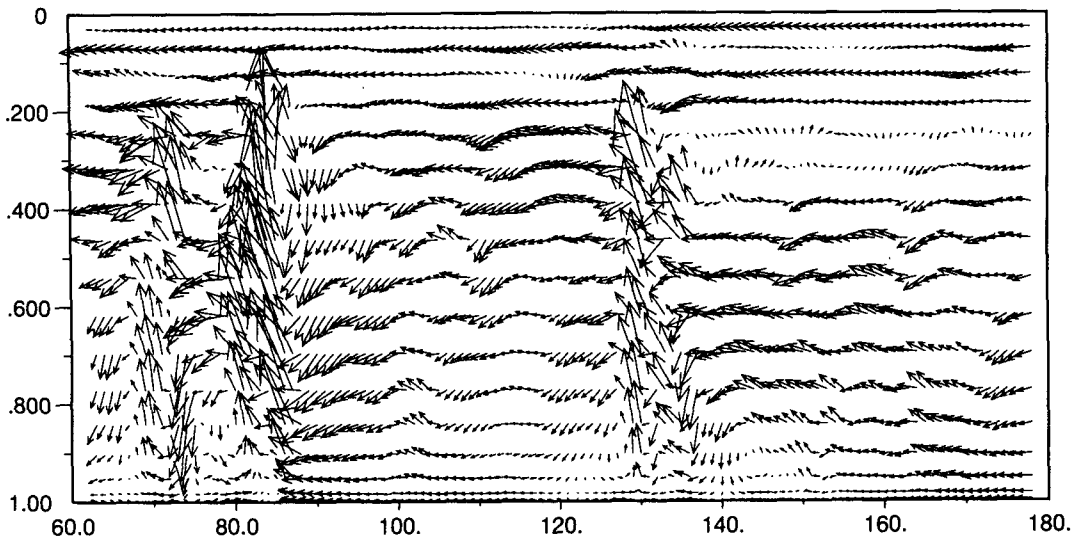

FIG. 2. Wind vector distribution of the control experiment at hour 6 of day 16. The maximum upward wind component located at 380 mb, 84° has a magnitude of 15.5×10^{-3} mb s^{-1}. The maximum westerly zonal wind component located at 280 mb, 86° has a magnitude of 7.8 m s^{-1}. The abscissa is longitude and the ordinate is height in sigma coordinate.

In the control experiment, SCS is used and so is the Rayleigh friction method of constraining the zonal wind. The Coriolis force is not employed. Figure 1 shows the time–longitude precipitation rate of the control. The cloud clusters have a size of about 300–400 km, a very realistic result. They last for about 3 days, and before the termination of a cloud cluster, a new cloud cluster forms about 1000 km to the east. This repeated generation of a new cloud cluster to the east of the existing cloud clusters, which soon terminate, gives rise to an envelope, a super cloud cluster, moving eastward. The super cloud cluster terminates when reaching the low SST domain; at any time there can be more than one super cloud cluster. The super cloud cluster covers a distance of 120° longitude in about 50 days, a speed in good agreement with the observed speed of the convective region associated with TISO, which travels from the Indian Ocean to mid-Pacific, a distance of about 120°, in about the same period. Thus, we have successfully, at least in a qualitative sense, simulated the cloud cluster life cycle, the super cloud cluster and its life cycle, and arguably the TISO in the

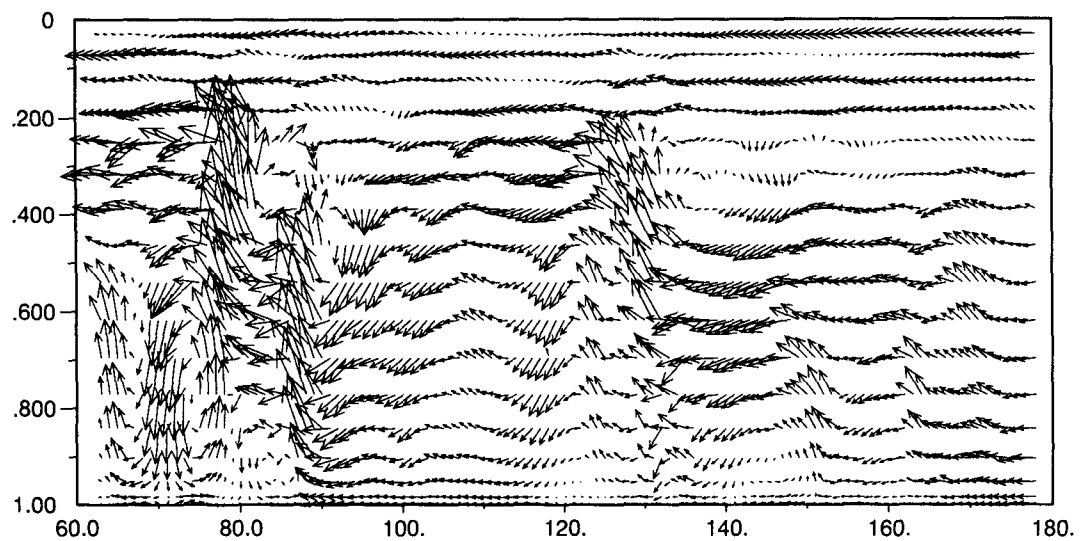

FIG. 3. Same as Fig. 2 six hours later.

present 2D model. The zonal mean wind is a vertically constant westward 10 m s^{-1} initially. Although the Rayleigh friction tries to maintain it at -10 m s^{-1}, surface friction reduces it to about -4 m s^{-1} near the surface in the first few days. Such reduction should slow down the westward movement of the cloud clusters. Thus, the faster westward cloud cluster speed after a few days must be attributed to the instability growth toward a greater moisture supply, as proposed later in this section in the discussion associated with Fig. 10. Parenthetically, the same experiment repeated with a 30-minute interval for the SCS rendered no qualitative difference in precipitation pattern, and the speeds of the cloud clusters and the super cloud cluster did not have noticeable changes.

In the mature phase of an existing cloud cluster, a downdraft of the cloud cluster scale forces the boundary-layer air to move eastward on the east side of the cloud cluster. Figure 2 shows the wind arrows of day 16, hour 6. A downward motion in the lower troposphere is located at 140°. This downward motion, as a part of the life cycle evolution of the cloud cluster centered over 132°, pushes the flow in boundary to its east eastward. This westerly creates a boundary-layer convergence that initiates a new cloud cluster at 150°, to the east of the existing cloud cluster. Six hours later the rising of the new cloud cluster is well under way (Fig. 3).

In SCS the convective instability starts from the lower troposphere and then moves up into the upper troposphere due to the upward transport of moisture and the rising large-scale motion. At the final stage of the cloud clusters the bulk of the convective instability is occurring in the mid- and upper troposphere. Rain reevaporation in the lower troposphere leads to net cooling and large-scale downdraft.

In the Introduction we pointed out the existence of the cloud cluster teleinduction mechanism and proposed that it is responsible for the origin of the super cloud cluster. Also, we proposed that the super cloud cluster is the main driving force of the tropical intraseasonal oscillations. The present results lend support for these proposed ideas.

In the above experiment the zonally averaged convective heating is largely balanced by the prescribed radiative cooling rate, since the zonally averaged vertical motion is zero, whereas in the real tropics the balance is largely due to Hadley circulation. To account for the effects of the zonal mean upward motion field missing in the model, zonally uniform heating and moistening rates (hereafter referred to as Hadley forcings) are prescribed in the next experiment. The heating component is set as $Q_H = Q_0 \sin(\pi p/1000)$, where p is pressure in mb and $Q_0 = -1$°C/day. The moistening component is set as $M_H = -\omega(\partial[\bar{q}]/\partial p)$, where $\omega = \omega_0 \sin(\pi p/1000)$, $\omega_0 = -2.0 \times 10^{-4}$ mb s^{-1}, and $[\bar{q}]$ is obtained from the Newell et al. time–zonal mean q. This cooling rate together with the radiative cooling rate determine the sum of the total cumulus heating and surface sensible heat flux in the model quasi-equilibrium state. This rather simple method of incorporating radiation and effects of zonal mean upward motion of the Hadley circulation is considered to be sufficient for our present limited purposes. Figure 4 shows the time–longitude precipitation in the experiment with the Hadley forcings. Due to the additional forcing the convective activity is more rigorous and there are three super cloud clusters. Also, the amplitude of the super cloud clusters is more steady.

We should point out that the strength that we specified for the Hadley forcings is somewhat excessive considering the fact that a large component of the Hadley upward motion occurs in three stationary locations, Amazon, Indonesia, and Northern Africa, and only part of the remaining amount is associated with the super cloud clusters. However, this excessive strength has the advantage of demonstrating that the super cloud clusters appearing in our model are quite robust with respect to the Hadley forcings. In the remaining experiments the Hadley forcings are not used.

Figure 5 shows the time–longitude precipitation for an experiment in which the rain reevaporation in SCS is not allowed. Besides demonstrating that rain reevaporation is not crucial for the existence of super cloud clusters in the model, the results show an interesting 7-day fluctuation of the amplitude of the super cloud clusters. The vertical heating profile in this experiment does not show cooling in the mature phase of the cloud clusters.

We also repeated the control experiment replacing SCS with the Emanuel convection scheme with a calling frequency of 15 min. The time–longitude precipitation result is shown in Fig. 6. It shows the 3-hourly accumulated precipitation (as in all precipitation figures in this paper). The precipitation has grid-size concentration, and most concentrations last for less than 3 hours. There is discontinuity in both time and space. This means that there is a high rate of precipitation within the 3 hour interval part of the three hours has no rain, and in the next three hours rain occurs in a neighboring grid usually on the eastern side. Such precipitation discontinuity is due to the fact that this scheme (if not by itself, at least when combined with the rest of our model, the boundary-layer treatment in particular) produced convective overadjustment. Overadjustment means that the convection scheme changes the T and q profiles to such a degree that the large-scale processes, even under their normal favorable conditions, cannot bring the profiles back to satisfy the convection initiation criterion before the next call of the convection scheme, and several convection calls have to elapse before the criterion can be met again. The consequence of overadjustment is spotty grid-size precipitation pattern, lacking continuity in both time

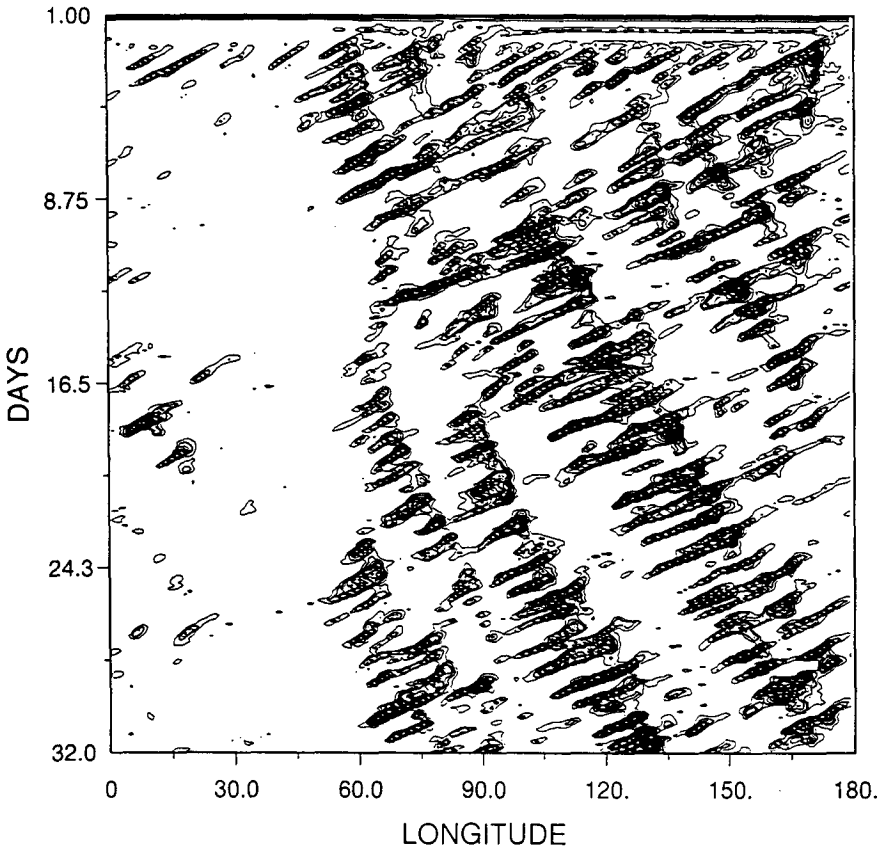

FIG. 4. Same as Fig. 1 but with Hadley forcings.

and space. The grid-size convection and the overadjustment must have contributed to the fact that cloud clusters did not appear in the experiment. Without cloud cluster, simulation of super cloud cluster and TISO is of course not possible. The grid-size convection is concentrated in a sizable region (30°–40° longitude) that moves eastward at a speed equivalent to circling the globe in 10–12 days, a common feature appearing in many aquaplanet simulations (Hayashi and Sumi 1987; Numaguti and Hayashi 1991; etc.). Such a feature is in good agreement with the wave–CISK interpretation of the TISO and is clearly not in agreement with observations. The eastward movement that appears in this 2D model certainly cannot be interpreted as Kelvin wave–CISK. It is probably due to the fact that the basic wind (and thus moisture supply) comes from the east, and thus new precipitation centers appear only to the east of the existing convective region. Whether this scheme or the way it is coupled to the rest of the model (involving changes outside this scheme) can be modified to generate cloud cluster and to simulate the cloud cluster teleinduction mechanism remains an interesting question.

The experiment with the relaxed Arakawa–Schubert scheme (with a calling frequency of every 9 minutes) did produce cloud clusters. However, the life cycle of the cloud clusters and the cloud cluster teleinduction mechanism were not successfully simulated. Thus, no super cloud cluster appeared. The precipitation (Fig. 7) shows patterns moving eastward similar to what the Emanuel scheme produced, although the detailed pattern is very different. The speed of the movement is typical of wave–CISK type simulation—much higher than that of observed super cloud clusters. In addition, the maximum precipitation is much lower than the control.

The experiment with the GFDL version of the moist convective adjustment yields results qualitatively very similar to those of the control (Fig. 8). The speed of the super cloud clusters is almost the same as that in the control. The separation between cloud clusters is very clear, and the life span of individual cloud cluster is somewhat longer than that in the control. Also the maximum precipitation intensity is much higher than that in the control. There are one to possibly three (around day 15) wave packets. The number of itera-

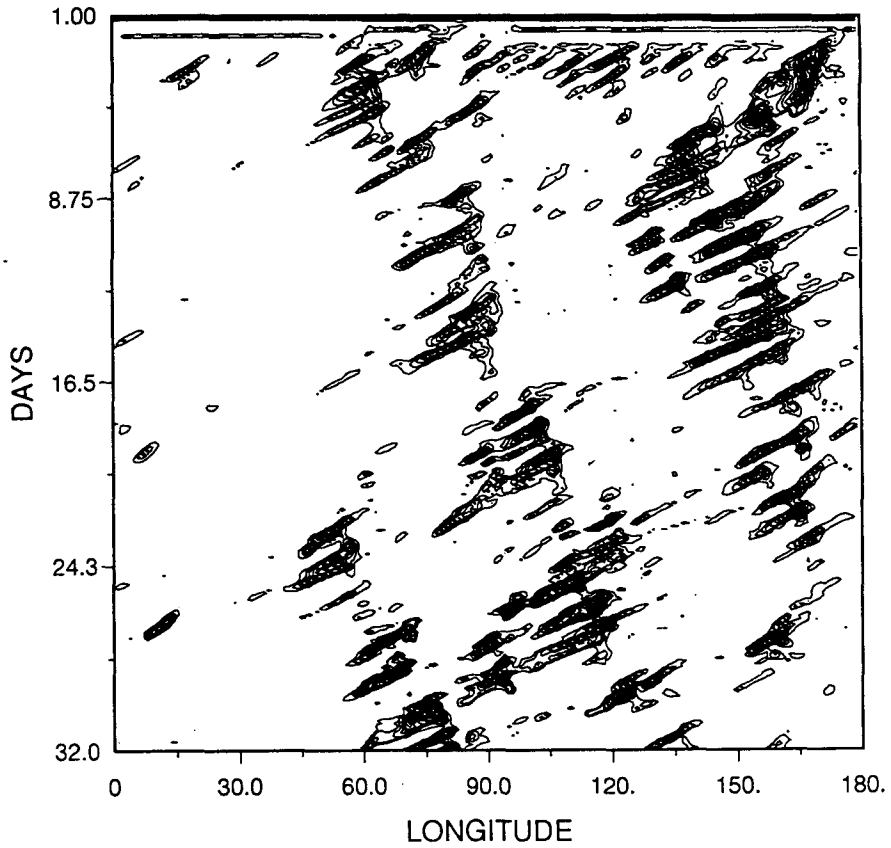

FIG. 5. Same as Fig. 1 but without rain reevaporation.

tions to bring the vertical temperature and humidity profile close to that of the moist adiabat every time the scheme is called can affect the precipitation pattern. The super cloud cluster pattern disappears, if three iterations per call are used. Additionally, the convection calling frequency can also significantly change the details of the precipitation pattern. With a higher calling frequency (9 minutes), the results show shorter cloud cluster life span and shorter distance between cloud clusters, though the speeds of the cloud clusters and the super cloud clusters change little. Figure 8 shows the results with one iteration and a calling frequency of one hour.

We did not try the Kuo scheme in our experiments. Judging from the fact that Hayashi and Sumi (1987) and Numaguti and Hayashi (1991), using the Kuo scheme, obtained results in agreement with the Kelvin wave–CISK mechanism, we expect that the Kuo scheme will not be successful.

Figure 9 shows the precipitation in an experiment repeating the control but with the Coriolis force term set at its value at 10°N. Also added in this experiment is a zonally uniform meridional pressure gradient force geostrophically balancing the zonal mean u wind. For simplicity the method of achieving this is a simple restoration of zonally averaged v wind on sigma surface to zero at every time step. That the zonal average is done on the sigma surfaces poses no serious problem in our no-topography setting. The super cloud clusters no longer exist and the life span of the cloud clusters is somewhat shortened. This result is consistent with the observational finding that TISO has largest amplitude right at the equator (Madden and Julian 1972).

The control experiment was also repeated with the Rayleigh friction–type method of constraining the zonally averaged u wind replaced by the method of restoring zonally averaged u wind to a vertically uniform constant of -5 m s^{-1} at every time step. This experiment provides a sensitivity test on the Rayleigh friction time scale, which is zero in this case. Figure 10 shows the time–longitude distribution of precipitation. The super cloud clusters still exist, but their eastward speed is faster than in the control. Obviously this is due to the fact that the basic wind that Rayleigh friction tends to adjust to in the control experiment is an easterly of greater magnitude (-10 m s^{-1}). The cloud clusters move westward at a speed of 11.5 m s^{-1}, that is, a westward 6.5 m s^{-1} relative to the zonally averaged u

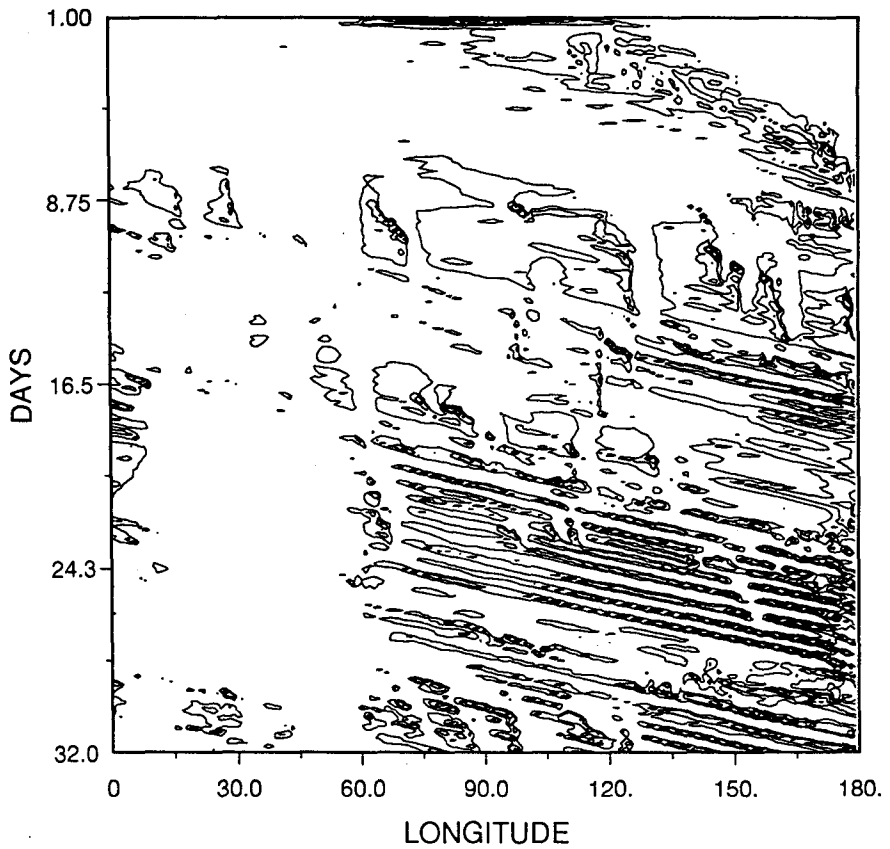

FIG. 6. Same as Fig. 1 but with SCS replaced by the Emanuel scheme.

wind. There is reason to believe this westward speed relative to the zonal mean wind is realistic. Nakazawa's (1988) Fig. 2 shows a cloud cluster westward speed of 16 m s^{-1} in the northern summer season. Judging from the Newell et al. analysis (their plate 3.14) of the climatological wind, the average easterly speed in the western Pacific is much less than 16 m s^{-1} in the lower troposphere. Thus, observations do show a westward speed relative to the basic flow for the cloud clusters. Such relative speed is consistent with the fact the new cloud clusters appearing in the east and competing for moisture supply with the existing ones. Thus, for the existing cloud clusters to maximize their moisture supply, it is better for them to assume a westward speed relative to the basic flow.

Summarizing our experimental results, we would conclude that our experiments support our interpretation of the origin of the TISO. One of our most important findings is that the successful simulation of the TISO depends critically on the choice of convection scheme. Specifically, the successful simulation of TISO depends on the model's ability to simulate the super cloud clusters, which in turn depends on the model's ability to simulate cloud clusters, their life cycle, and the cloud cluster teleinduction mechanism. The latter phenomena depend critically on the choice of convection scheme for their successful simulation.

4. Discussion

One of the most intriguing questions arising from our experiments is what in a convection scheme is so critical for the successful simulation of the life cycle of the cloud clusters and the successful simulation of the super cloud clusters (including the cloud cluster teleinduction mechanism), which drive the TISO. This is a very fundamental question and is of great importance. Our speculative answer is that schemes such as RAS and Kuo's keep the state of the model atmosphere away from not only the critical point where vertical profile becomes grid-scale convectively unstable but also the critical point where the cloud cluster teleinduction mechanism can occur, and thus do not possess the ability to simulate the life cycle of cloud clusters. In the case of RAS the model atmosphere is constantly adjusted to an observed average equilibrium state, characterized by a constant cloud work function for each cloud type, which is not very close to the convective

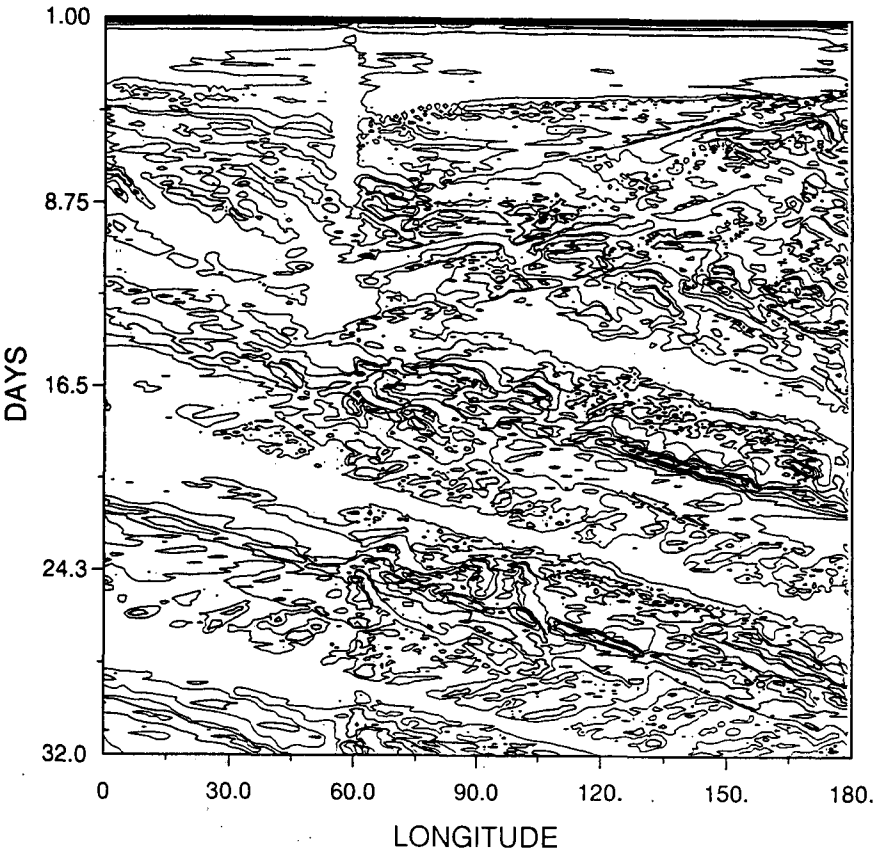

FIG. 7. Same as Fig. 1 but with SCS replaced by RAS.

instability critical point. The constant cloud work functions for different cloud types are obtained from observed tropical soundings. These sounding profiles are of course the results of convective instabilities of various scales including cloud, cloud cluster, and super cloud cluster scales. Therefore, RAS keeps the model atmosphere to an equilibrium state that corresponds to the resultant state of various convective instabilities. In other words, RAS is already doing what these instabilities are trying to achieve, and thus prevents the model from exhibiting phenomena due to these instabilities. This is the same as the fact that dry convective adjustment prevents the models from exhibiting dry convection. In the Kuo scheme, convection is invoked as long as there is any moisture convergence in an atmospheric column. So the criterion for convection to occur is not tied to a grid-scale moist convectively unstable profile.

On the other hand, the schemes such as ours and the moist convective adjustment scheme only keep the model atmosphere away from the grid-scale moist convective instability and allow the state of atmosphere to exceed the critical point for cloud cluster instability. In these schemes, adjustment is done when the temperature and moisture profiles are grid-scale moist convectively unstable and the amount of adjustment is only sufficient to remove such instability; thus, the ability for the model atmosphere to simulate linear and nonlinear cloud cluster instabilities is intact. At this writing, we are not certain whether the Emanuel scheme can be successful when its overadjustment problem is resolved.

Our study touches upon the basic strategy of cumulus parameterization. If the purpose of cumulus parameterization is to simulate the effects of grid-scale moist convective instability, then it is best to do just that. Doing more would mean the likelihood of suppressing or distorting convective instability of larger scales. It can thus lead to unphysical modes such as the wave–CISK mode that is found in our experiments with RAS and the Emanuel scheme and in many previous 3D experiments with the Kuo scheme. Of course, when constructing a new cumulus convection scheme it may not be easy to judge from the design whether or not the scheme will exclude or distort the linear and nonlinear cloud cluster instabilities. A simple 2D model like ours provides a good preliminary test-bed. Taking a broader view, we should also point out that a quali-

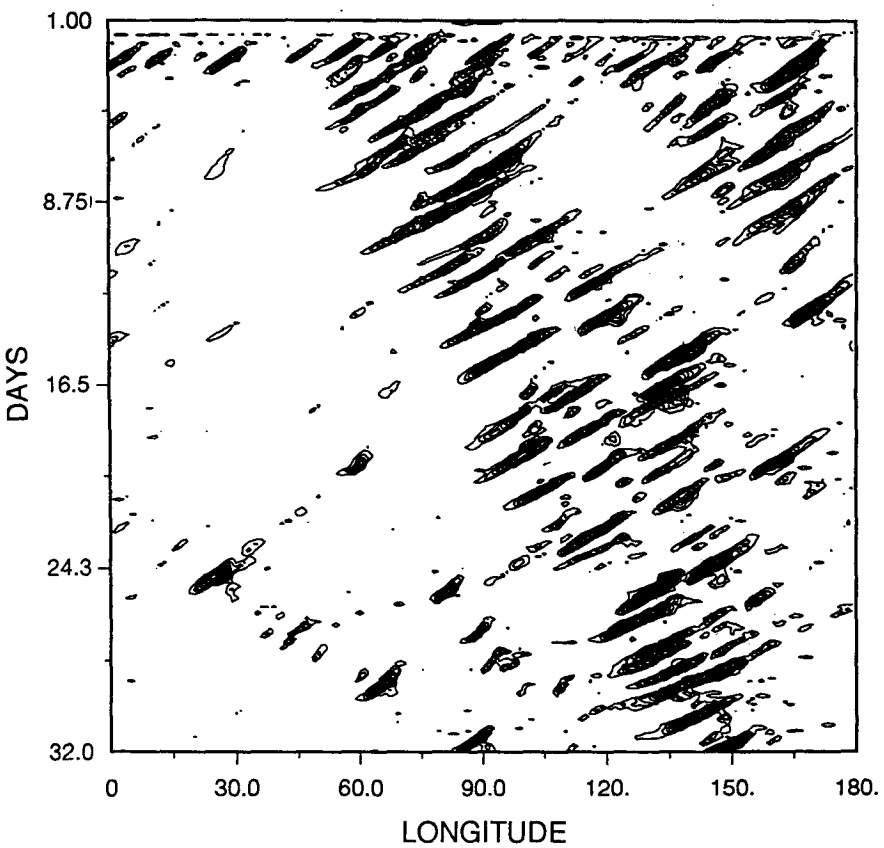

FIG. 8. Same as Fig. 1 but with SCS replaced by the moist convective adjustment scheme.

tative successful simulation of TISO is only one of the criteria in measuring the success of a convection scheme. The quantitative successful simulation of TISO and the successful simulation the quasi equilibrium of the tropical atmosphere are also important criteria.

From what we have simulated and what exists in observations, we would like to point out a formal analogy between the super cloud clusters and the middle-latitude finite amplitude baroclinic wave packets (Pedlosky 1972). Although the cloud cluster instability is entirely different from the baroclinic instability, the upstream cloud cluster teleinduction mechanism is analogous to the downstream cyclogenesis in the middle-latitude wave packets, both at the front of the packet. Using this wave packet analogy, it is not hard to understand that there can be more than one super cloud cluster existing at the same time. The number of wave packets appearing in a quasigeostrophic model can be increased by raising the supercriticality of baroclinic instability (Lee and Held 1993). Similarly, our experiment with the Hadley forcing (Fig. 2) has more super cloud clusters than the control. The cause for the middle-latitude wave packets is the nonlinear baroclinic instability, or the finite-amplitude baroclinic instability. Analogously, the cause for the super cloud cluster must be the nonlinear cloud cluster instability. Based on this analogy, we would also suggest that super cloud clusters are, in their canonical form, really solitary waves. As shown by Pedlosky (1972), these wave packets owe their existence to both linear and nonlinear instabilities, and their speed is *not* that of the group velocity (a linear concept) of the carrier waves (the middle-latitude cyclones or the cloud clusters in our case).

Though it is easy to infer superficially that the speed of the super cloud clusters is related to that of the basic flow, the frequency of cloud cluster generation, and the distance between cloud clusters, a derivation of an analytical expression for the speed parallel to Pedlosky's (1972) work would be much more interesting and informative. Also using the middle-latitude baroclinic wave packets, which interact with the background flow, as a guide, it is reasonable to expect TISO to interact with zonal mean wind. Such interaction may lead to fluctuation of the zonal mean wind in the 40–50-day period as observed (Anderson and Rosen 1983) as well as fluctuation of the total intensity of the train of super cloud clusters. Our 2D model, due to the way we force

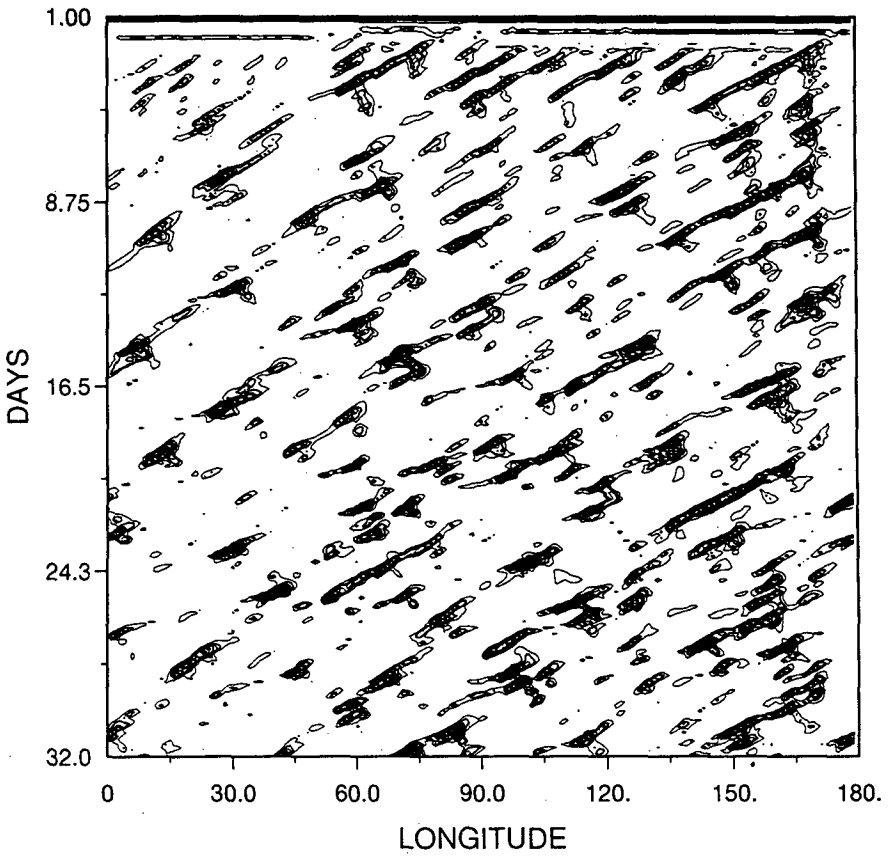

FIG. 9. Same as Fig. 1 but with the Coriolis term set at its value at 15°N.

the zonal mean flow, hinders such interaction. This restriction will disappear when we go to the 3D model. An aspect that our 2D model fails to achieve is that observations (Fig. 5 of Nakazawa 1988) show super cloud clusters tend to pack together to form a convective region. This is also likely related to the way we force the zonal mean flow. We anticipate that the 3D model will show improvement in this aspect.

At a more fundamental level, in order to be complete our interpretation for the TISO should also include the origin for the cloud clusters, that is, the cloud cluster instability, both in its linear and nonlinear forms. The importance of the cloud cluster instability for the tropics rivals that of the baroclinic instability for the middle latitudes. The basic ideas in wave–CISK and WISHE of cooperation among convective heating, heating-induced circulation, and circulation-enhanced surface fluxes provide good basis for studying the cloud clusters. This instability along with the life cycle, the size, and the internal structure of the cloud clusters is currently being intensively studied by the research community.

5. Summary and remarks

In summary, we have put forth a new framework for interpreting the origin of TISO. Our interpretation takes into account the recent observational facts related to super cloud clusters, and it avoids the speed and scale selection problems that have long plagued the previous theories. In supporting our interpretation, we have simulated in a 2D model the tropical intraseasonal oscillation, including the super cloud cluster, the life cycle of cloud cluster, and the cloud cluster teleinduction mechanism. These simulation results demonstrate that the core of the origin of the TISO is the cloud cluster teleinduction mechanism, which is responsible for the existence of the super cloud clusters, and that the successful simulation of these multiscale phenomena depends critically on the cumulus convection scheme used. Moreover, we have provided a speculative answer for what distinguishes the successful cumulus convection schemes from the unsuccessful ones.

Our findings are of course all based on the 2D simulation. The circulation associated with the TISO in the

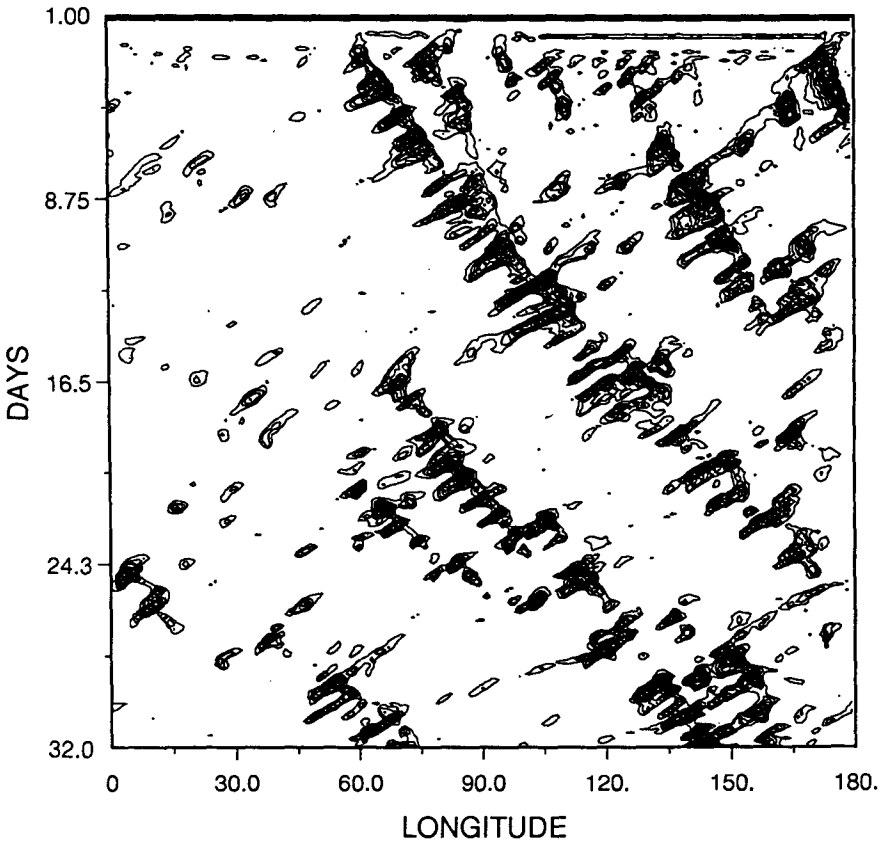

FIG. 10. Same as Fig. 1 but with the Rayleigh friction–type method of constraining the zonally averaged u wind replaced by the method of restoring zonally averaged u wind to a vertically uniform constant of -5 m s^{-1} at every time step.

2D model is convectively forced gravity wave on both sides of the super cloud cluster. In a 3D model we expect the super cloud cluster to excite Kelvin wave to its east and Rossby wave to its west (Chao 1987), and the eastward propagation of the TISO is not directly linked to the speeds of these two waves. The successful 2D simulation indicates that horizontal wind shear is not necessary in the cloud cluster teleinduction mechanism. However, horizontal wind shear can still play a supporting role in 3D models and in nature.

The GFDL convective adjustment scheme has produced results very similar to those based on the simple convective scheme. Thus, as long as the cumulus scheme does no more than removing the grid-scale convective instability, TISO can be successfully simulated. The details of the convective scheme, such as rain reevaporation, are not crucial, although they do affect the details of the life cycle of the cloud clusters. Which of these two schemes and what modifications in them can give the best details of the cloud cluster teleinduction mechanism will have to be studied with the aid of observations, such as the TOGA COARE data. The sudden rise of the new cloud cluster suggests a catastrophe phenomenon whose details may lead to interesting insights.

Our 2D model suffers from the limitation of not having Kelvin and Rossby waves. Thus, another of our future directions is naturally the numerical simulation of the tropical intraseasonal oscillation and the related phenomena in a 3D GCM. Our present work has clearly demonstrated the importance of cumulus convection scheme in this investigation. Thus, we will try our convection scheme and the moist convective adjustment scheme in the 3D model. A successful simulation of TISO should produce not only a power spectrum peak in the 40–50-day range in various fields but also the movement of super cloud clusters from the Indian Ocean to the mid-Pacific in the same time range.

There are more problems associated with the TISO that we have not touched upon. The movement of the TISO convection region from the Indian Ocean to the western Pacific is not always very smooth. In northern summer the movement is occasionally very abrupt with the appearance of a convection seesaw (Zhu and Wang

1993). Also in northern summer there is northward movement of a northwest–southeast band shape convective region in the Indian Ocean and the India subcontinent (Yasunari 1981). Furthermore, spectral analysis of ECMWF data (Hayashi and Golder 1993) shows a distinct tropical tropospheric planetary 25–30 day oscillation that has weaker amplitude than the 40–50-day wave. These phenomena require additional investigations and will be a part of our future research.

Acknowledgments. We thank K. A. Emanuel for providing the code for his convection scheme and S. Manabe and R. J. Stouffer for providing the GFDL moist convective adjustment scheme code. K.-M. Lau provided valuable moral support in launching the project that supported this work. Financial support from NASA Earth Science and Applications Division as a part of NASA participation in the TOGA COARE program was indispensable.

REFERENCES

Anderson, J. R., and R. D. Rosen, 1983: The latitude–height structure of 40–50 variations in atmospheric angular momentum. *J. Atmos. Sci.*, **40**, 1584–1591.

Arakawa, A., and M. J. Suarez, 1983: Vertical differencing of the primitive equations in sigma coordinates. *Mon. Wea. Rev.*, **111**, 34–35.

Chang, C.-P., and H. Lim, 1988: Kelvin wave–CISK: A possible mechanism for the 30–50 day oscillations. *J. Atmos. Sci.*, **45**, 1709–1720.

Chao, W. C., 1987: On the origin of the tropical intraseasonal oscillation. *J. Atmos. Sci.*, **44**, 1940–1949. Corrigendum, **45**, p. 1832.

Emanuel, K. A., 1987: An air–sea interaction model of intraseasonal oscillation in the tropics. *J. Atmos. Sci.*, **44**, 2324–2340.

——, 1991: A scheme for representing cumulus convection in large-scale models. *J. Atmos. Sci.*, **21**, 2313–2335.

Fox-Rabinovitz, M., M. Helfand, A. Hou, L. Takacs, and A. Molod, 1991: Numerical experiments on forecasting climate simulation and data assimilation with the new 17 layer GLA GCM. Preprints, *9th Conf. on Numerical Weather Prediction,* Denver, Amer. Meteor. Soc., 506–509.

Hayashi, Y., and D. G. Golder, 1993: Tropical 40–50 and 25–30 day oscillations appearing in realistic and idealized GFDL climate model and the ECMWF dataset. *J. Atmos. Sci.*, **50**, 464–494.

Hayashi, Y. Y., and A. Sumi, 1986: The 30–40 day oscillations simulated in an "aqua-planet" model. *J. Meteor. Soc. Japan,* **64**, 451–467.

Hendon, H. H., 1988: A simple model of the 40–50 day oscillation. *J. Atmos. Sci.*, **45**, 569–584.

Kalnay, E., R. Balgovind, W. Chao, D. Edelmann, J. Pfaendtner, L. Takacs, and K. Takano, 1983: Documentation of the GLAS fourth-order general circulation model. Vol. 1: Model Documentation, NASA Tech. Memo 86064. [Available from NASA/GSFC, Greenbelt, MD 20771.]

Lau, K.-M., and P. H. Chen, 1986: The 40–50 day oscillation and the El Niño/Southern Oscillation: A new perspective. *Bull. Amer. Meteor. Soc.*, **67**, 533–534.

——, and L. Peng, 1987: Origin of low-frequency (intraseasonal) oscillations in the tropical atmosphere. Part I: Basic theory. *J. Atmos. Sci.*, **44**, 950–972.

——, ——, C. H. Sui, and T. Nakazawa, 1989: Dynamics of super cloud clusters, westerly wind burst, 30–60 day oscillations and ENSO: A unified view. *J. Meteor. Soc. Japan,* **67**, 205–219.

——, T. Nakazawa, and C. H. Sui, 1991: Observations of cloud cluster hierarchies over the tropical western Pacific. *J. Geophys. Res.*, **96**(Suppl.), 3197–3208.

Lee, S., and I. M. Held: 1993: Baroclinic wave packets in models and observations. *J. Atmos. Sci.*, **50**, 1413–1428.

Lin, S.-J., W. C. Chao, Y. C. Sud, and G. K. Walker, 1994: A class of the van Leer–type transport schemes and its application to the moisture transport in a general circulation model. *Mon. Wea. Rev.*, in press.

Louis, J.-F., 1979: A parametric model of vertical eddy fluxes in the atmosphere. *Bound.-Layer Meteor.*, **17**, 187–202.

Madden, R. A., 1986: Seasonal variations of the 40–50 day oscillation in the tropics. *J. Atmos. Sci.*, **24**, 3138–3158.

——, and P. R. Julian, 1971: Detection of a 40–50 day oscillation in the zonal wind in the tropical Pacific. *J. Atmos. Sci.*, **28**, 702–708.

——, and ——, 1972: Description of global scale circulation cells in the tropics with a 40–50 day period. *J. Atmos. Sci.*, **29**, 1109–1123.

Manabe, S., J. Smagorinsky, and R. F. Strickler, 1965: Simulated climatology of a general circulation model with a hydrological cycle. *Mon. Wea. Rev.*, **93**, 769–798.

Miyahara, S., 1987: A simple model of the tropical intraseasonal oscillation. *J. Meteor. Soc. Japan,* **65**, 341–351.

Moorthi, S., and M. J. Suarez, 1992: Relaxed Arakawa–Schubert: A parameterization of moist convection for general circulation models. *Mon. Wea. Rev.*, **120**, 978–1002.

Murakami, T., and T. Nakazawa, 1985: Tropical 40–50 day oscillations during the 1979 northern hemisphere summer. *J. Atmos. Sci.*, **42**, 1107–1122.

Nakazawa, T., 1988: Tropical super clusters within intraseasonal variations over the western Pacific. *J. Meteor. Soc. Japan,* **66**, 823–839.

Neelin, J. D., I. M. Held, and K. H. Cook, 1987: Evaporation–wind feedback and low-frequency variability. *J. Atmos. Sci.*, **44**, 2341–2348.

Newell, R. E., J. W. Kidson, D. G. Vincent, and G. J. Boer, 1972: *The General Circulation of the Tropical Atmosphere and Interactions with Extratropical Latitudes,* Vol. 2. The MIT Press, 371 pp.

Nogues-Paegle, J., B.-C. Lee, and V. E. Kousky, 1989: Observed modal characteristics of the intraseasonal oscillation. *J. Climate,* **2**, 496–507.

Numaguti, A., and Y.-Y. Hayashi, 1991: Behavior of cumulus activity and the structures of circulations in an "aqua planet" model. Part 1. The structure of the super clusters. *J. Meteor. Soc. Japan,* **69**, 541–561.

Pedlosky, J., 1972: Finite-amplitude baroclinic wave packets. *J. Atmos. Sci.*, **29**, 680–686.

Rui, H., and B. Wang, 1990: Development characteristics and dynamic structure of tropical intraseasonal convection anomalies. *J. Atmos. Sci.*, **47**, 357–379.

Sud, Y. C., and A. Molod, 1988: The roles of dry convection, cloud–radiation feedback processes and the influence of recent improvements in the parameterizations in the GLA GCM. *Mon. Wea. Rev.*, **116**, 2366–2387.

Sui, C.-H., and K.-M. Lau, 1992: Multiscale phenomena in the tropical atmosphere over the western Pacific. *Mon. Wea. Rev.*, **120**, 407–430.

Takahashi, M., 1987: A theory of the slow phase speed of the intraseasonal oscillation using wave–CISK. *J. Meteor. Soc. Japan,* **65**, 43–49.

Wang, B., 1988: Dynamics of tropical low-frequency waves: An analysis of the moist Kelvin wave. *J. Atmos. Sci.*, **45**, 2051–2065.

——, and J.-K. Chen, 1989: On the zonal scale selection and vertical structure of the equatorial intraseasonal waves. *Quart. J. Roy. Meteor. Soc.*, **115**, 1301–1323.

——, and H. Rui, 1990: Dynamics of the coupled moist Kelvin–Rossby wave on an equatorial β-plane. *J. Atmos. Sci.,* **47,** 397–413.

Yamagata, T., and Y. Hayashi, 1984: A simple diagnostic model for the 30–50 day oscillation in the tropics. *J. Meteor. Soc. Japan,* **62,** 709–717.

Yano, J.-I., and K. Emanuel, 1991: An improved model of the equatorial troposphere and its coupling with the stratosphere. *J. Atmos. Sci.,* **48,** 377–389.

Yasunari, T., 1981: Structure of an Indian summer monsoon system with around 40 day period. *J. Meteor. Soc. Japan,* **59,** 336–354.

Yoshizaki, M., 1991: On the selection of eastward-propagating modes appearing in the wave–CISK model. *J. Meteor. Soc. Japan,* **69,** 595–608.

Zhu, B., and B. Wang, 1993: The 30–60-day convection seesaw between the tropical Indian and western Pacific Oceans. *J. Atmos. Sci.,* **50,** 184–199.